

# Single Image Dehazing with White Balance Correction and Image Decomposition

Renjie He<sup>\*†</sup>, Zhiyong Wang<sup>†</sup>, Hao Xiong<sup>†</sup> and David Dagan Feng<sup>†</sup>

<sup>\*</sup>Northwestern Polytechnical University, Xian 710072, China

<sup>†</sup>School of Information Technologies, The University of Sydney, Australia

Email: davidhrj@gmail.com, zhiyong.wang@sydney.edu.au, hxio4690@uni.sydney.edu.au, dagan.feng@sydney.edu.au

**Abstract**—Single image dehazing has been a challenging problem due to its ill-posed nature. While most of the existing single image based dehazing algorithms address this issue by introducing certain assumptions and priors into the haze imaging model, the imaging process of imaging devices has been seldom taken into account, such as white balance and metering. In general, consumer photos are taken with AWB (Auto White Balance). Hence, color temperature in a foggy scenario may not be correctly detected, which results in color distortion; and the whole scene looks brighter, which leads to under-exposure during the imaging process. In this paper, we propose to handle these two issues by applying white balance correction and decomposing an image into two component images, reflex lightness image and ambience illumination image. We devise an improved dark channel prior based algorithm to dehaze the reflex lightness image and the exposure adjustment is estimated from the ambience illumination image. Finally, a high quality haze-free image is produced by refining the brightness of the preliminarily dehazed image with the estimated exposure adjustment. Experimental results with a benchmark dataset demonstrate that our approach outperforms the state-of-the-art, in terms of contrast and color fidelity.

## I. INTRODUCTION

The phenomena such as haze, fog and smoke are mainly contributed by the increased size of particles in the atmospheric medium which affect atmospheric absorption, emission and scattering of lights. As a result, outdoor scenery images of these scenarios are often of low visual quality (e.g. low contrast) as shown in Fig. 1(a). Therefore, dehazing is highly desired for improving visual quality (as shown in Fig. 1(b)), which is beneficial for both consumers and computer vision applications. It is also helpful to obtain depth information of a scene in the dehazing process [1].

Nayar and Narasimhan [2] introduced a dichromatic atmospheric scattering model to describe hazy images by formulating the observed pixel values  $I(\mathbf{x})$  (i.e. hazed pixel value) of location  $\mathbf{x}$  as the contribution from two parts: the scene radiance  $J(\mathbf{x})$  reflecting the light from the captured scene and the global atmospheric light  $A$  (i.e. environmental illumination including sunlight, diffused skylight, and light reflected from the ground). The model is mathematically described as below:

$$I(\mathbf{x}) = J(\mathbf{x})t(\mathbf{x}) + A(1 - t(\mathbf{x})). \quad (1)$$

Note that  $t(\mathbf{x})$  is the medium transmission describing the portion of the light that reaches the camera without scattering [3] and generally expressed as:

$$t(\mathbf{x}) = e^{-\beta d(\mathbf{x})}, \quad (2)$$



Fig. 1. A sample of single image based dehazing. Left: input hazy image. Right: haze-free image produced by our approach.

where  $\beta$  is the scattering coefficient of the atmosphere medium and  $d$  is the scene depth. That is, the scene radiance is attenuated exponentially with the scene depth.

The goal of dehazing is to recover  $J$ ,  $A$ , and  $t$  from  $I$ , which is an ill-posed problem, since there is insufficient information to solve Equation (1). In general, attempts to such a challenging problem are categorized into two groups, multi-source based approaches and single image based approaches. The approaches of the former category rely on multiple images or extra information. In [4][5], images taken of the same scene with different degrees of polarization were utilized for haze removal. In [6], multiple images were taken in different weather conditions for this purpose. In [1][7], depth information was provided from user inputs or a known 3D model. While the methods mentioned above can achieve good results, the extra information required is often not easily available.

Single image based dehazing approaches (i.e. the latter category) rely on certain assumptions or prior knowledge. Tan [8] proposed to remove haze by maximizing local image contrast of an input image since haze-free images are generally of high contrast. Due to its lack of physical ground, dehazed images appear over-saturated. Fattal [9] proposed to obtain the medium transmission by estimating the albedo of a scene under the assumption that the transmission and surface shading are locally uncorrelated. Though being physically reasonable, this approach has limitation with heavy haze regions where

the different components are difficult to resolve. Kratz and Nishino [10] imposed natural statistics priors on both the depth and albedo values and jointly estimated the depth and albedo through a canonical probabilistic formulation. However, the results are prone to halo and color distortion. Tarel *et al* [11] introduced constraints on the depth variation by maximizing the atmospheric veil assuming that it must be smooth most of the time. Carr and Hartley [12] applied a camera geometry prior to transmission refinement by assuming that depth increases from bottom to top. Recently, He *et al* [13] proposed a novel exploitation of the dark channel prior which is based on the observation and statistics of outdoor haze-free images.

While these approaches focus on the scattering model and different assumptions, imaging devices (e.g. cameras) have been seldom taken into account. With the advances in digital imaging, consumer photos are often taken with Auto White Balance (AWB) and Auto Exposure (AE) settings. Hence, color temperature in a foggy scenario may not be correctly detected, which results in color distortion; and the whole scene looks brighter, which leads to under-exposure during the imaging process. In this paper, we aim to address these two issues in single image dehazing.

In order to correct white balance, we estimate the airlight with the dark channel prior, as the airlight refers to the most hazy region which is white. By setting the airlight to pure white, each color channel is stretched to ensure the color accuracy of the image. In order to obtain exposure adjustment, we propose to decompose an input image into two component images: ambience illumination image and reflex lightness image, so as to estimate ambient illumination from the ambience illumination image. For the reflex lightness image, we propose to improve the dark channel prior based approach with refined transmission estimation. Finally, a high quality haze-free image is produced by refining the brightness of the preliminarily dehazed image with the estimated exposure adjustment. An overview diagram of the proposed approach is illustrated in Fig. 2.

The remaining of this paper is organized as follows. In Section II, the key steps of our approach for single image haze removal are introduced in detail. In section III, the experimental results are reported and discussed. Finally, in Section IV, the conclusion is presented.

## II. THE PROPOSED ALGORITHM

As illustrated in Fig. 2, our proposed approach consists of the following steps: white balance correction, image decomposition, transmission map estimation and refinement, and enhancement, exposure adjustment estimated from the ambience illumination image, and producing haze-free image by taking both preliminarily dehazed image and exposure adjustment information into account.

### A. White Balance Correction

The human visual system (HVS) is capable of reliably interpreting object colors with surrounding illumination. In the photographic process, this ability is simulated with the

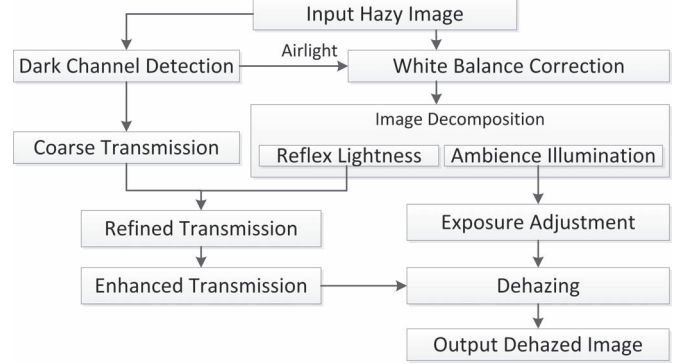


Fig. 2. Illustration of the proposed approach.

white balance function which helps identify the reference of white color for accurate color production. Without a proper white balance, photos taken by cameras may show undesirable color cast. In order to ensure the natural color reproduction of scenes, AWB of cameras generally relies on the estimation of color temperature. Color temperature refers to the color appearance of the light that comes from a light source. For example, higher color temperature implies a colder (more blue) light while lower color temperature implies a warmer (more red) light [14]. Objects in a hazy scene usually have higher color temperature, which may cause unrealistic color casts. In order to correct the color, we apply white balance correction prior to dehazing by calibrating the fog color to pure white.

In Tan's work [8], the pixel with the highest intensity value is chosen as the airlight, under the assumption that these pixels represent an object at infinite distant. He *et al* [13] took pixels with brightest dark channel values as the most hazy pixels and chose the one with highest intensity among these pixels as the airlight. Fattal [9] computed the airlight by solving an optimization problem. Since precise estimation of the airlight plays an important part in the correction process, we employ He's method [13] in our approach.

Similar to He's method [13], the airlight is determined provided that the dark channel of the patch is bright and the patch is in the upper part of an image. In this paper, we choose the value from the top 0.1% brightest and the top 25% height pixels in the dark channel as the airlight. Dark channel of a haze-free image in [13] can be defined mathematically as a minimum value operation in patches around the target pixel as follows:

$$J^{\text{dark}}(\mathbf{x}) = \min_{y \in \Omega(\mathbf{x})} \left( \min_{c \in \{r,g,b\}} J^c(y) \right), \quad (3)$$

where  $J^{\text{dark}}(\mathbf{x})$  represents the dark channel of the pixel located at  $\mathbf{x}$ ,  $J^c$  is a color channel of  $J$  and  $\Omega(\mathbf{x})$  is the local patch centred at  $\mathbf{x}$ .

Assuming that the input image  $I(x)$  is normalized between 0 and 1, the procedure of white balance implies that the intensity of the airlight  $A$  can be set to pure white, and the rest part of image can be normalized as follow:

$$\tilde{I}^c = \mathbf{W}I^c, \quad (4)$$



Fig. 3. A sample of white balance correction. Left: original image. Right: white balance corrected image.

where  $\tilde{I}$  and  $I$  represent the corrected image and the input hazy image, respectively,  $c \in \{r, g, b\}$  is color channel index.  $\mathbf{W} = \text{diag}(W^r, W^g, W^b)$  is the scale matrix, and each channel of  $\mathbf{W}$  is defined as:

$$W^c = \frac{A^c}{\max^c}. \quad (5)$$

As shown in Fig. 3, the input hazy image looks bluish, apparently, the image after white balance correction looks more natural and the airlight is corrected to white.

### B. Image Decomposition

The in-camera metering is standardized based on the luminance of the light which would be reflected from an object appearing as middle gray, which varies around 10-18% gray. Middle gray is commonly accepted because a typical scene generally reflects the same amount of light as this gray value [14].

The in-camera metering works well if object reflectance is sufficiently diverse throughout the scene. In other words, if there is an even spread varying from dark to light objects, the average reflectance will be approximately middle gray. However, there may be a significant imbalance of subject reflectivity in some scenes (e.g. a hazy scene). As a result, these scenes are often under-exposed with in-camera metering.

Therefore, in order to obtain accurate luminance of the light, we decompose the input image into reflex lightness image and ambience illumination image with the following equations [15]:

$$I^c(\mathbf{x}) = RL^c(\mathbf{x}) + AL^c(\mathbf{x}) \quad (6)$$

$$RL^c(\mathbf{x}) = (1 - \kappa) \cdot I^c(\mathbf{x}) \quad (7)$$

$$AL^c(\mathbf{x}) = \kappa \cdot I^c(\mathbf{x}) \quad (8)$$

where  $I^c(\mathbf{x})$  is the color channel  $c$  of the input hazy image,  $RL^c(\mathbf{x})$  and  $AL^c(\mathbf{x})$  represent the reflex lightness image and the ambience illumination image, respectively, and  $\kappa$  is a weighting factor.

In general, weighting factor  $\kappa$  satisfies the following criterion: A bright area in the ambience illumination image remains brighter than a dark area and after the ambience illumination is removed, the left part keeps the original sequence of the brightness. Hence,  $\kappa$  is defined as:

$$\kappa = \frac{1}{2} \frac{I(\mathbf{x})}{I_{\max}}, \quad (9)$$



Fig. 4. A sample of image decomposition. Left: reflex lightness image. Right: ambience illumination image.

where  $I_{\max}$  is the maximum pixel value.

As shown in Fig. 4, through image decomposition, the ambience illumination image preserves illumination information and the reflex lightness image preserves the color and content details. In this paper, the reflex lightness image is utilized to improve the dark channel prior based dehazing and ambience illumination image is utilized to estimate the exposure adjustment.

### C. Transmission Map Estimation

1) *Coarse Estimation*: In order to obtain the transmission  $t$ , we employ the method proposed in [13]. We firstly rewrite Equation (1) as follows:

$$t(\mathbf{x}) = 1 - \frac{I(\mathbf{x}) - J(\mathbf{x})}{A - J(\mathbf{x})} \quad (10)$$

Applying the dark channel prior to Equation (10), we have the new patch transmission  $\tilde{t}(\mathbf{x})$  (assumed to be constant within the local patch) as:

$$\tilde{t}(\mathbf{x}) = 1 - \frac{I^{\text{dark}}(\mathbf{x}) - J^{\text{dark}}(\mathbf{x})}{A - J^{\text{dark}}(\mathbf{x})}. \quad (11)$$

According to the dark channel prior, the dark channel value of scene radiance  $J$  is low and tends to be zero [13] mainly due to three reasons: a) shadows, b) colourful objects or surfaces, and c) dark objects or surfaces. That is,

$$J^{\text{dark}}(\mathbf{x}) = \min_{y \in \Omega(\mathbf{x})} \left( \min_{c \in \{r, g, b\}} J^c(y) \right) \rightarrow 0, \quad (12)$$

where  $\Omega(\mathbf{x})$  is a local patch and  $c$  is the color channel.

Since the airlight  $A$  is positive, the transmission  $\tilde{t}(\mathbf{x})$  is computed as follows:

$$\tilde{t}(\mathbf{x}) = 1 - \min_{y \in \Omega(x)} \left( \min_{c \in \{r, g, b\}} \left( \frac{I^c(y)}{A^c} \right) \right). \quad (13)$$

The second column of Fig. 5 shows the coarse estimation of transmission maps with patch size  $11 \times 11$ . As can be seen, the extracted transmission map contains halos and block effects since the transmission is not always constant in a patch. Therefore, the coarse transmission map needs to be refined.

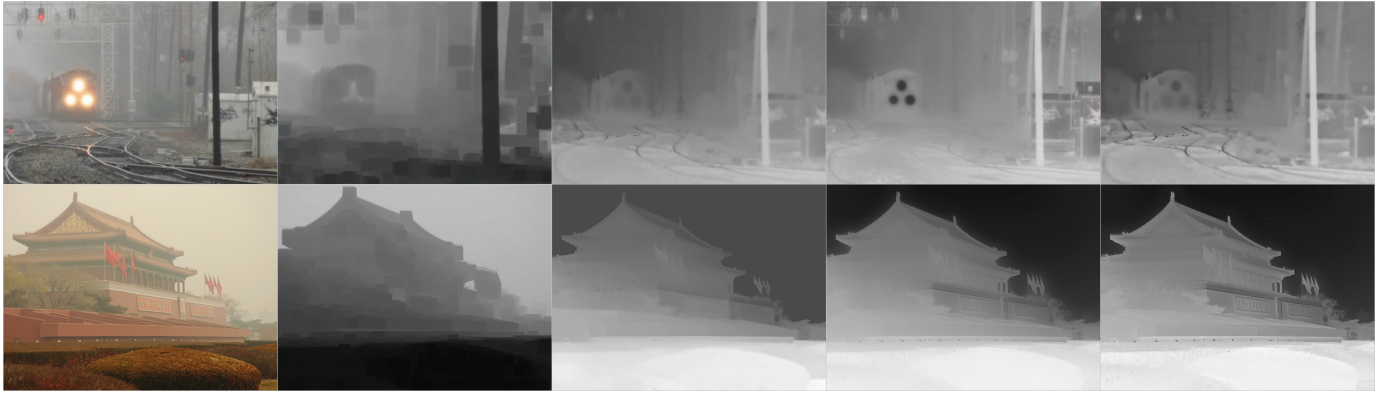


Fig. 5. Sample results of transmission map estimation. From left to right: hazy image, dark channel, refined transmission map with soft matting [13], our refined transmission map with the guided filter, our enhanced transmission map.

2) *Transmission Map Refinement*: Different methods have been proposed to refine the coarse transmission map. In [9], Fattal used Gaussian-Markov random field model [16] guided by the input image to extrapolate the solution to the whole image. However, this method is computationally intensive. In [13], the author used soft matting method [17] to refine the transmission map, which is also time consuming. In [18], the author proposed to refine the transmission map with a cross-bilateral filter. However, it has been noticed that the bilateral filter may have the gradient reversal artefacts in detailed decomposition. In this paper, we refine the coarse transmission map  $\tilde{t}$  using the guided image filter [19] due to its effectiveness and efficiency.

As mentioned in [13], the transmission map is refined by solving a sparse linear system:

$$(\mathbf{L} + \lambda \mathbf{U})t = \lambda \tilde{t}, \quad (14)$$

where  $\mathbf{L}$  is the matting Laplacian matrix proposed in [17],  $\mathbf{U}$  is an identity matrix of the same size as  $\mathbf{L}$ , and  $\lambda$  is a regularization parameter. The elements of the matting Laplacian matrix [17] are defined as:

$$L_{ij} = \sum_{k:(i,j) \in \omega_k} \left( \delta_{ij} - \frac{1}{|\omega|} \left( 1 + \frac{(I_i - \mu_k)(I_j - \mu_k)}{\sigma_k^2 + \tau} \right) \right), \quad (15)$$

where  $I_i$  and  $I_j$  are the colors of input image  $I$  at pixels  $i$  and  $j$ ,  $\mu_k$  and  $\sigma_k^2$  are the mean and the variance of  $I$  in window  $\omega_k$ , respectively.  $|\omega|$  is the number of pixels in window  $\omega_k$ .  $\tau$  is the regularization parameter and  $\delta_{ij}$  is the Kronecker delta.

As noticed that the kernel of guided filter in [19] has similar form with the elements of the matting Laplacian matrix, therefore, Equation (15) can be represented by the guided filter kernel weight  $W_{ij}$  as:

$$L_{ij} = |\omega| (\delta_{ij} - W_{ij}). \quad (16)$$

The guided filter kernel weight  $W_{ij}$  is defined as follow:

$$W_{ij}(I) = \frac{1}{|\omega|^2} \sum_{k:(i,j) \in \omega_k} \left( 1 + \frac{(I_i - \mu_k)(I_j - \mu_k)}{\sigma_k^2 + \tau} \right), \quad (17)$$

where  $I$  is the guidance image. The refined transmission map is obtained by substituting Equation (17) into Equation (15) and Equation (14).

As shown in Fig. 5, the refined transmission map obtained with the guided filter (the third column) has more details, compared with the result obtained with the soft matting (the fourth column) [13]. In addition, guided filter based refinement is faster than the soft matting based refinement. For a computer with an Intel Xeon W3520 processor, it takes less than 0.1 second on average to process a  $800 \times 600$  image using the guided filter while it takes approximately 15 seconds using soft matting on average.

3) *Transmission Map Enhancement*: After the above refinement, the transmission map is smoothed. In order to extract more details from the transmission map, the guided filter is further applied in this paper to enhance the refined transmission map, since it avoids the gradient reversal artefacts.

As an image can be modelled as the combination of a smooth layer and a detailed layer, the refined transmission map is rewritten as:

$$t = L^{\text{smooth}} + L^{\text{detail}}. \quad (18)$$

That is, image details are able to be extracted by amplifying the detailed layer. In Equation (17), when  $\delta_k^2 \ll \tau$ , the guided filter kernel becomes a low-pass filter:

$$W_{ij}(I) = \frac{1}{|\omega|^2} \sum_{k:(i,j) \in \omega_k} 1. \quad (19)$$

Therefore, the refined transmission map is firstly smoothed with edge-preserving filter as a smooth layer  $L^{\text{smooth}}$  as:

$$L^{\text{smooth}} = \sum_j W_{ij}(t) t, \quad (20)$$

then the detailed layer  $L^{\text{detail}}$  is obtained as the difference between the refined transmission map and the smooth layer,

$$L^{\text{detail}} = t - L^{\text{smooth}}. \quad (21)$$

The enhanced transmission map is finally computed as:

$$t^{\text{enhanced}} = L^{\text{smooth}} + \gamma L^{\text{detail}}, \quad (22)$$

where  $\gamma$  is the amplification coefficient, to prevent the detail being over-amplified,  $\gamma$  is set as 1.7 in this paper.

As shown in the fifth column of Fig. 5, the enhanced transmission map better captures the sharp edge discontinuities and outlines the profile of the objects, compared with the refined transmission map.

#### D. Dehazing

With the enhanced transmission map, the scene radiance can be obtained by directly solving the inverse of Equation (1)

$$J(\mathbf{x}) = \frac{I(\mathbf{x}) - A}{t_m} + A, \quad (23)$$

where  $t_m = \max(t^{\text{enhanced}}(\mathbf{x}), 0.1)$  since  $J(\mathbf{x})t(\mathbf{x})$  in Equation (1) can be very close to zero.

#### E. Exposure adjustment

As mentioned in Section II-B, due to the under-exposure for foggy scenes in the imaging process, dehazed images generally appear dim. In this paper, we propose to enhance the dehazed image by utilizing the ambience illumination image. Note that other advanced enhancement algorithms can also be integrated into our decomposition framework so as to take advantage of the ambient illumination image.

As ambience illumination image is always brighter than reflex lightness image, we modify the brightness of scene radiance to the level of ambience illumination image, which is shown as follows,

$$J' = J \frac{\log(\overline{AL} + \varepsilon)}{\log(\overline{RL})}, \quad (24)$$

where  $J'$  denotes the adjusted image and  $J$  is the scene radiance obtained in Section II-D,  $\overline{AL}$  and  $\overline{RL}$  denote the mean of the ambience illumination image and the reflex lightness image, respectively,  $\varepsilon$  is a small constant which is set to 0.03 based on our experiments and observations in this paper. That is, the brightness of the scene radiance is adjusted to the median value of the ambience illumination image as close as possible.

### III. EXPERIMENTAL RESULTS

In this section, we present the experimental results with the benchmark dataset [11] which also provides dehazing results of the state-of-the-art approaches, including Tan's [8], He's [13], Tarel's [11] and Kopf's [20] for the comparison with our proposed approach. Evaluation of our proposed approach is demonstrated both qualitatively and quantitatively.

#### A. Qualitative Evaluation

Since our approach mainly relies on the dark channel prior based dehazing method [13], we firstly compare our approach with He's work [13] as shown in Fig. 6. The upper two images were used for conducting experiments in [12]. As observed in the first row, our result (the third column) outperforms He's result (the second column) in terms of both visibility and rich details, particularly around the cargo area. For the second sample shown in the second row, the clear difference



Fig. 6. Qualitative comparison with He's work [13]. Left: input hazy image. Middle: He's result. Right: our result.

between our result and He's result is that the color of our result is more realistic, while the color of He's result is a bit yellowish due to the dust in the air. This is due to the advantage of the white balance correction. The visibility of the dehazed image obtained with our approach is also enhanced significantly. Even in very dense haze condition, as can be seen in the third row, since the color of the plane is similar to the atmospheric light and less shadow is cast in the image, color distortion appeared under the plane in He's result. Our approach is able to unveil the rich details. Additionally, due to the higher color temperature, the sky of hazy image appears bluish. It can be seen from the right image that the dehazed image has the proper color.

We provide further qualitative comparison with other popular single image dehazing algorithms by using two benchmark images (one city view image shown in Fig. 7(a) and one landscape image shown in Fig. 8(a)). As observed from Figs. 7 and 8, the dehazing results of our approach have a better balance of color accuracy, visibility, and proper overall brightness. Specifically, as shown in both Figs. 7(b) and 8(b), histogram equalization may cause excessive enhancement and result in color distortion, as the white cloud appears yellowish. As shown in Figs. 7(c) and 8(c), Fattal's results are visually satisfactory. However, his method requires sufficient color information and variance. Hence, in the situation of dense fog, this algorithm may be unreliable on estimating the transmission due to the insufficient variance. Figs. 7(d) and 8(d) show the results using Tan's method. As can be seen that the color of Tan's result is over-saturated due to the overestimation of the haze layer. Kopf's results in Figs. 7(e) and 8(e) show a clear boundary between sky and the land. However, their approach requires 3D geometric information and the texture maps of the scene. He's results, as shown in Figs. 7(f) and 8(f), remove the haze effectively. However the results generally look dim. In addition, in Fig. 8(f), the edge of the cloud appears yellowish. Figs. 7(g) and 8(g) show Tarel's results. His algorithm reduces the haze effect of the

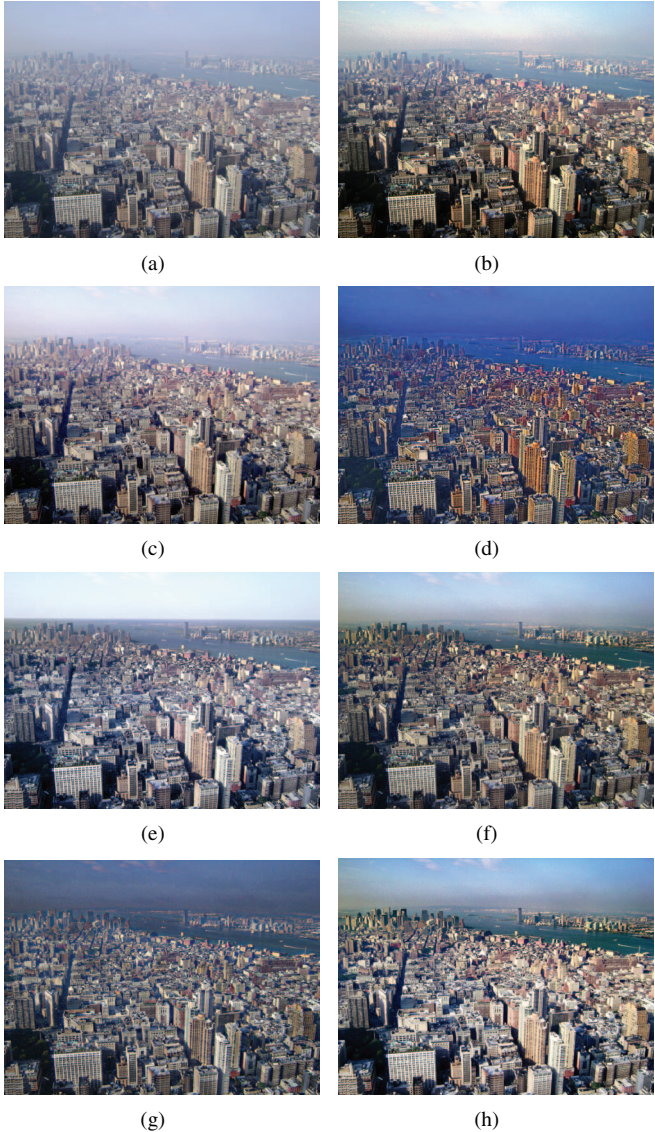


Fig. 7. A dehazing sample of a city view image. (a) Input hazy image. (b) Histogram equalization. (c) Fattal's result [9]. (d) Tan's result [8]. (e) Kopf's result [20]. (f) He's result [13]. (g) Tarel's result [11]. (h) our result.

input image. However, the results are distorted by halos, which can be seen around the cloud in Fig. 8(g).

### B. Quantitative Evaluation

To quantitatively evaluate our algorithm, we use the blind contrast enhancement assessment metric proposed by Tarel *et al* [11]. Three indicators  $e$ ,  $\bar{r}$  and  $\sigma$  are computed in the evaluation for comparing the input hazy image and the processed image, where  $e$  represents the rate of edges newly visible after enhancement,  $\bar{r}$  estimates the average visibility enhancement obtained by the enhancement algorithm, and  $\sigma$  is the percentage of pixels that becomes completely black or completely white after dehazing. A better dehazed image is generally supposed to have higher values of  $e$  and  $\bar{r}$  and lower value of  $\sigma$ .

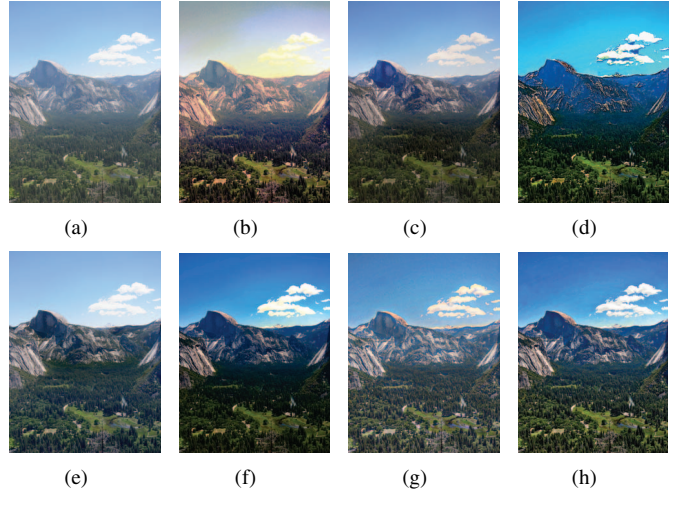


Fig. 8. A dehazing sample of a landscape image. (a) Input hazy image. (b) Histogram equalization. (c) Fattal's result [9]. (d) Tan's result [8]. (e) Kopf's result [20]. (f) He's result [13]. (g) Tarel's result [11]. (h) our result.

Tables I and II show the quantitative performance for Fig. 7(a) and Fig. 8(a), respectively. It is observed from  $e$  that our result has more visible edges due to the transmission enhancement and lightness adjustment. Although Tan's result has slightly higher value of  $\bar{r}$  for the city view image, edges seem to be over enhanced as shown in Fig. 7(d). In addition, our method is able to achieve the smaller percentage of pixels which become completely black or completely white after dehazing.

TABLE I  
QUANTITATIVE EVALUATION FOR THE CITY VIEW IMAGE (FIG. 7)

Fig. 7	$e$	$\bar{r}$	$\sigma$
Histogram Equalization	0.03	1.79	0.02
Fattal's[9]	0.09	1.54	0.24
Tan's[8]	0.02	<b>2.17</b>	0.44
Kopf's[20]	0.01	1.61	0.08
He's[13]	0.02	1.63	0.01
Tarel's[11]	0.01	1.87	<b>0</b>
Ours	<b>0.18</b>	2.16	<b>0</b>

TABLE II  
QUANTITATIVE EVALUATION FOR THE LANDSCAPE IMAGE (FIG. 8)

Fig. 8	$e$	$\bar{r}$	$\sigma$
Histogram Equalization	0.01	1.29	0.03
Fattal's[9]	0.04	1.23	0.15
Tan's[8]	0.08	2.28	0.05
Kopf's[20]	<b>0.09</b>	1.62	0.02
He's[13]	0.08	1.33	0.07
Tarel's[11]	0.02	2.09	<b>0</b>
Ours	<b>0.09</b>	<b>2.84</b>	0.01

## IV. CONCLUSION & DISCUSSION

In this paper, we present an approach to improve single image based dehazing by taking the imaging process of imaging devices into account. Firstly, white balance correction is utilized to eliminate color distortion of an input hazy

image. Secondly, we decompose the input hazy image into the reflex lightness image and ambience illumination image so that exposure information can be handled separately to improve the quality of the final dehazed image. In addition, transmission map estimated with the dark channel prior is refined and enhanced with the guided filter. By refining the initially dehazed image with appropriate exposure adjustment, a high quality haze-free image is produced. Experimental results of the images from a benchmark dataset demonstrated that our proposed approach is able to preserve better color accuracy and visibility. In our future work, we will further investigate the integration of the decomposition model with the scattering model.

#### ACKNOWLEDGMENT

The work presented in this paper was partially funded by Natural Science Foundation of China, and by ARC (Australian Research Council). The first author is sponsored by CSC (China Scholarship Council). The authors would like to thank the anonymous reviewers for their constructive comments.

#### REFERENCES

- [1] S. Narasimhan and S. Nayar, "Interactive (de) weathering of an image using physical models," in *Proceedings of IEEE Workshop on Color and Photometric Methods in Computer Vision*, 2003, pp. 1–8.
- [2] S. Nayar and S. Narasimhan, "Vision and the atmosphere," *International Journal of Computer Vision*, vol. 48, no. 3, pp. 233–254, 2002.
- [3] B. Xie, G. Fan, and Z. Cai, "Improved Single Image Dehazing Using Dark Channel Prior and Multi-scale Retinex," in *Proceedings of International Conference on Intelligent System Design and Engineering Application*, vol. 1, 2010, pp. 848–851.
- [4] Y. Schechner, S. Narasimhan, and S. Nayar, "Instant dehazing of images using polarization," in *Proceedings of IEEE International Conference on Computer Vision and Pattern Recognition*, 2001, pp. 325–332.
- [5] S. Shwartz, E. Namer, and Y. Schechner, "Blind Haze Separation," in *Proceedings of IEEE International Conference on Computer Vision and Pattern Recognition*, 2006, pp. 1984–1991.
- [6] S. Nayar and S. Narasimhan, "Vision in bad weather," in *Proceedings of IEEE International Conference on Computer Vision*, vol. 2, 1999, pp. 820–827.
- [7] K. Tan and J. Oakley, "Enhancement of color images in poor visibility conditions," in *Proceedings of IEEE International Conference on Image Processing*, vol. 2, 2000, pp. 788–791.
- [8] R. Tan, "Visibility in bad weather from a single image," in *Proceedings of IEEE International Conference on Computer Vision and Pattern Recognition*, 2008, pp. 1–8.
- [9] R. Fattal, "Single image dehazing," *ACM Transactions on Graphics*, vol. 27, no. 3, pp. 1–9, 2008.
- [10] L. Kratz and K. Nishino, "Factorizing scene albedo and depth from a single foggy image," in *Proceedings of IEEE International Conference on Computer Vision*, 2009, pp. 1701–1708.
- [11] J. Tarel and N. Hautiere, "Fast visibility restoration from a single color or gray level image," in *Proceedings of IEEE International Conference on Computer Vision*, 2009, pp. 2201–2208.
- [12] P. Carr and R. Hartley, "Improved single image dehazing using geometry," in *Proceedings of International Conference on Digital Image Computing: Techniques and Applications*, 2009, pp. 103–110.
- [13] K. He, J. Sun, and X. Tang, "Single image haze removal using dark channel prior," in *Proceedings of IEEE Conference on Computer Vision and Pattern Recognition*, 2009, pp. 1956–1963.
- [14] B. Stoppe, *Stoppees' Guide to Photography and Light*, Mar. 2010.
- [15] B. Li, S. Wang, and Y. Geng, "Image enhancement based on Retinex and lightness decomposition," in *IEEE International Conference on Image Processing*, 2011, pp. 3417–3420.
- [16] P. Perez, "Markov random fields and images," *Centrum voor Wiskunde en Informatica Quarterly*, vol. 11, no. 4, pp. 413–437, 1998.
- [17] A. Levin, D. Lischinski, and Y. Weiss, "A Closed-Form Solution to Natural Image Matting," *IEEE Transactions on Pattern Analysis and Machine Intelligence*, vol. 30, no. 2, pp. 228–242, 2008.
- [18] X. Lv, W. Chen, and I. Shen, "Real-Time Dehazing for Image and Video," in *Proceedings of Pacific Conference on Computer Graphics and Applications*, 2010, pp. 62–69.
- [19] K. He, J. Sun, and X. Tang, "Guided image filtering," in *Proceedings of the European Conference on Computer vision: Part I*, 2010, pp. 1–14.
- [20] J. Kopf, B. Neubert, B. Chen, M. Cohen, D. Cohen Or, O. Deussen, M. Uyttendaele, and D. Lischinski, "Deep photo: Model-based photograph enhancement and viewing," *ACM Transactions on Graphics*, vol. 27, no. 5, pp. 1–10, 2008.